HHS Public Access

Author manuscript

NMR Biomed. Author manuscript; available in PMC 2017 May 01.

Published in final edited form as:

NMR Biomed. 2016 May ; 29(5): 650–659. doi:10.1002/nbm.3509.

Hyperpolarized ^{13}C lactate-to-bicarbonate ratio as a biomarker for monitoring acute response of anti-VEGF treatment

Jae Mo Park[a], **Daniel M. Spielman**[a], **Sonal Josan**[a,b], **Taichang Jang**[c], **Milton Merchant**[c], **Ralph E. Hurd**[d], **Dirk Mayer**[b,e], and **Lawrence D. Recht**[c]

[a]Department of Radiology, Stanford University, 1201 Welch Rd., Stanford, California 94305, U.S.A

[b]Biosciences Division, SRI International, 333 Ravenswood Ave.., Menlo Park, California 94025, U.S.A

[c]Department of Neurology and Neurological Sciences, Stanford University, 875 Blake Wilbur Dr., Palo Alto, California 94304, U.S.A

[d]Applied Science Laboratory West, GE Healthcare, 333 Ravenswood Ave., Menlo Park, California 94025, U.S.A

[e]Department of Diagnostic Radiology and Nuclear Medicine, , University of Maryland, 22 S. Greene St., Baltimore, Maryland 21201, U.S.A

Abstract

Hyperpolarized [1-^{13}C]pyruvate MRS provides a unique imaging opportunity to study reaction kinetics and enzyme activities of *in vivo* metabolism both because of its favorable imaging characteristics as well as its critical position in the cellular metabolic pathway where it can either be reduced to lactate (reflecting glycolysis) or converted to acetyl-CoA and bicarbonate (reflecting oxidative phosphorylation).

Cancer tissue metabolism is altered in such a way as to result in a relative preponderance of glycolysis as compared to oxidative phosphorylation (i.e., Warburg effect). While there is a strong theoretical basis for presuming that readjusting the metabolic balance towards normal could alter tumor growth, a robust noninvasive *in vivo* tool with which to measure the balance between these two metabolic processes has yet to be developed.

Until recently, hyperpolarized ^{13}C-pyruvate imaging studies have focused solely on [1-^{13}C]lactate production because of its strong signal. However, without a concomitant measure of pyruvate entry into the mitochondria, the lactate signal provides no information on the balance between the glycolytic and oxidative metabolic pathways. Consistent measurement of ^{13}C-bicarbonate in cancer tissue, which does provide such information, has proven difficult, however.

In this study, we report reliable measurement of ^{13}C-bicarbonate production both in healthy brain and a highly glycolytic experimental glioblastoma model using an optimized ^{13}C MRS imaging protocol. With the capacity to obtain signal in all tumors, we also confirm for the first time that the ratio of ^{13}C-lactate-to-bicarbonate provides a more robust metric than does ^{13}C-lactate for

Corresponding Author: Jae Mo Park, Address: Department of Radiology, Stanford University, 1201 Welch Rd., Stanford, California 94305-5488, U.S.A. Phone: +1 (650) 504-1648, jaemo@stanford.edu.

assessing the metabolic effects of an anti-angiogenic therapy. Our data suggest a potential application of this ratio as an early biomarker to assess therapeutic effectiveness. Furthermore, although further study is needed, the results suggest that anti-angiogenic treatment results in a rapid normalization in the relative tissue utilization of glycolytic and oxidative phosphorylation by tumor tissue.

Keywords

hyperpolarized ^{13}C; angiogenesis; cancer therapy responses; bevacizumab; glioma

Introduction

Carbon-13 (^{13}C) magnetic resonance spectroscopy (MRS) has proven a useful noninvasive tool that provides *in vivo* measurements of bioenergetics due to its ability to assess key metabolites via ^{13}C-labeling of selected metabolic precursors. Conventional ^{13}C MRS, however, requires both a continuous infusion of the ^{13}C substrate to generate measureable steady-state signals and long acquisition times to overcome the low MR sensitivity.

Hyperpolarized ^{13}C MRS using dynamic nuclear polarization (DNP) provides a unique imaging opportunity to observe real-time *in vivo* metabolism, in effect enabling one to study reaction kinetics and enzyme activities[1,2]. ^{13}C-pyruvate labeled in C_1 position is a suitable candidate to investigate cellular energy metabolism because cells can take up pyruvate and oxidize it in the mitochondria via the tricarboxylic acid (TCA) cycle. Pyruvate can be enzymatically reduced to lactate in glycolysis (GLY) or converted to acetyl coenzyme A (acetyl-CoA) and carbon dioxide, detected *in vivo* as a bicarbonate ($H^{13}CO_3^-$) peak, as it enters the mitochondria where it can undergo oxidative phosphorylation (OXPHOS)[3]. ^{13}C-lactate detected following the administered hyperpolarized [1-^{13}C]pyruvate has been suggested as a biomarker of GLY, with measurements correlated with lactate dehydrogenase (LDH) activity and tissue NAD^+/NADH balance[4–7]. Pyruvate dehydrogenase (PDH) activity controls pyruvate flux into mitochondria by catalyzing the pyruvate-to-acetyl-CoA conversion. The released CO_2 rapidly equilibrates with bicarbonate, making ^{13}C-bicarbonate detection in a hyperpolarized ^{13}C-pyruvate experiment a surrogate marker for OXPHOS when acetyl-CoA conversion to non-TCA pathways (i.e., ketone body and fatty acid metabolism) are relatively low, as is the case for brain[8–10].

Cancer imaging is one of the most promising applications of hyperpolarized [1-^{13}C]pyruvate. Warburg first noted almost a century ago that cancer over-utilizes GLY relative to OXPHOS for energy needs even in the presence of adequate oxygenation (i.e., aerobic glycolysis)[11,12]; this relative preponderance of GLY has provided the theoretical underpinnings for positron emission tomography (PET) scanning and is now being applied to hyperpolarized ^{13}C MRS, where the lactate-to-pyruvate ratio has been successful in detecting cancer metabolism[13,14] and monitoring metabolic changes after anti-cancer treatments[15–17]. Imaging flux through the mitochondria has been more challenging, but is crucial if increasing OXPHOS relative to GLY impacts tumor growth. Indeed, a previous study using ^{13}C NMR isotopomer analysis in surgical samples reported that the tumors

oxidizes alternative substrates in the TCA cycle[18]. However, to date, because reliable tumor measurement of ^{13}C-bicarbonate is difficult, most hyperpolarized ^{13}C-pyruvate imaging studies in cancer have focused solely on [1-^{13}C]lactate production.[13,17,19].

In a prior study[20], we reported that it was possible to obtain measurements of ^{13}C-bicarbonate in highly glycolytic brain tumors, demonstrating a decreased lactate-to-bicarbonate ratio when pyruvate dehydrogenase kinase (PDK) was artificially inhibited using dichloroacetate (DCA)[21]. To assess whether this lactate-to-bicarbonate metric could be affected independent of direct alteration of the metabolic pathway, thus expanding the potential clinical application as well as introducing this metric itself as a possible biomarker, we next assessed the impact of vascular endothelial growth factor (VEGF) inhibition, an important clinical anti-cancer therapy. Currently, research into the pathophysiology of anti-angiogenic agents has been focused on how changes in vessel dynamics impact tissue oxygenation and blood flow with relatively little attention paid to metabolic alterations[22–24]. A recent study showed a correlation between vascular normalization and lactate-pyruvate flux through LDH using hyperpolarized [1-^{13}C]pyruvate and dynamic contrast enhanced (DCE) MRI in colorectal cancer xenograft models with anti-angiogenic treatment[16]. However, bicarbonate was not measured in this study and no assessment of mitochondrial utilization was reported.

In this study, we further demonstrate the robust acquisition of both ^{13}C-bicarbonate and ^{13}C-lactate metabolite maps in brain using hyperpolarized [1-^{13}C]pyruvate, and report the relative utility of the lactate/bicarbonate ratio for monitoring anti-VEGF response in glioma-bearing rats. Our findings indicate that the reciprocal relationship between lactate and bicarbonate provides additional insights into the effects of anti-angiogenic agents on tumor metabolism.

Experimental

Polarization procedure

Pyruvate samples, prepared by mixing 14-M [1-^{13}C]-labeled pyruvic acid (Sigma-Aldrich, St. Louis, MO, USA) and 15-mM trityl radical OX063 (Oxford Instruments Molecular Biotools, Oxford, UK), were polarized using a HyperSense DNP system (Oxford Instruments Molecular Biotools). A solvent buffer solution consisting of 40-mM tris(hydroxymethyl)aminomethane, 125-mM NaOH, 100-mg/L ethylenediaminetetraacetic acid (EDTA), and 50-mM NaCl was used for dissolution of the 125-mM hyperpolarized [1-^{13}C]pyruvate (pH = ~7.5). Liquid-state polarization at dissolution was calculated to be approximately 25 % based on solid-state measurements and independent calibration experiments[25].

Animal model and experimental set-up

Healthy (N = 3, body weight = 248–273 g) and C6 glioma-implanted (N = 43, 203–316 g) male Wistar rats were prepared for the study. Each animal was anesthetized with 1.5–3.0 % isoflurane in oxygen (~1.5 L/min) followed by tail vein catheterization and placement in a clinical 3T MR scanner (GE Healthcare, Waukesha, WI, USA) and high-performance insert

gradient coil[26]. Each animal received an intravenous tail vein administration of 2.6–3.8 mL of the 125-mM hyperpolarized [1-^{13}C]pyruvate solution, adjusted to maintain a dose of 1 mmol/kg body weight at a rate of 0.25 mL/s, followed by a flush of 0.5 mL of heparinized (1 %) saline to clear the catheter line. Vital signs, including respiration, heart rate, temperature, and oxygen saturation were monitored throughout the imaging experiments. Respiration was consistently maintained at ~60 breaths per minute by regulating isoflurane level[27], and body temperature was kept at ~37 °C using a warm water blanket placed underneath the animal. The local Institutional Animal Care and Use Committee approved all procedures and animal's care.

C6 glioma and anti-VEGF treatment

Intra-subject in vivo measurement—Tumors grow rapidly after implantation of 1 × 10^6 C6 glioma cells, derived from an N-methyl-N-nitrosourea (MNU)-induced tumor[28], into rat brain, resulting in symptoms generally requiring euthanasia by day 15. Since Avastin® (bevacizumab) does not bind to rat VEGF, making it unsuitable for studies on C6 glioma, we obtained another anti-VEGF mab, B20-4.1.1 (courtesy of Roche/Genentech) that was identified from antibody phage libraries and which binds and blocks human, rat and murine VEGF interaction with VEGF receptors VEGFR1 and VEGFR2 with high *in vitro* potency[29,30]. We assessed the impact of acute intraperitoneal administration of B20.4.1.1 (5 mg/kg) at baseline and 3 hrs after administration (N = 3, 220–236 g), to rats harboring tumors in their right striatum. A separate group of glioma-implanted rats (N = 3, 244–268 g) were also imaged using the hyperpolarized ^{13}C MRSI at baseline and 3 hrs after saline injection for comparison.

Group in vivo measurements—The hyperpolarized [1-^{13}C]pyruvate (125 mM) was injected into four groups of glioma-bearing rats (C6 cells implanted 10 days prior to the hyperpolarized ^{13}C imaging experiments) through a tail vein catheter: untreated (N = 15, 220–284 g) and treated rats at 3 hrs (N = 9, 212–244 g), 24 hrs (N = 8, 203–316 g), and 48 hrs (N = 8, 272–300 g) after a single injection of 20-fold diluted anti-VEGF mab (5 mg/kg). For the 48 hrs post-treatment group, anti-VEGF mab was injected 9 days after glioma implantation to avoid excessive growth of the tumor.

MR protocol

A custom-made ^{13}C/^{1}H dual-tuned quadrature radiofrequency (RF) coil (inner diameter = 50 mm) was used for MR excitation and data acquisitions. Single-shot fast spin echo (FSE) proton MR images were acquired for anatomical reference covering up to 45 slices in axial, coronal, and sagittal planes (pulse repetition time (TR)/echo time (TE) = 1492/38.6 ms, slice thickness = 2 mm, and in-plane resolution = 0.47 mm). A dual-echo T_2-weighted FSE sequence ($TR/TE_1/TE_2$ = 5000/11.3/56.7 ms, slice thickness = 1 mm, in-plane resolution = 0.25 mm, matrix size = 256 × 192, echo train length = 8, 25 slices, scan time = 8:05 min) in the axial plane was used to confirm the tumor location. The B_0 field was optimized with the linear shim currents to be spatially homogeneous over the imaging slice containing the tumor by minimizing the line width of the unsuppressed water signal from a point-resolved proton spectroscopy sequence.

Chemical shift imaging (CSI) sequence with four spatially interleaved spiral readouts (spectral bandwidth = 932.8 Hz, in-plane field of view (FOV) = 43.5 mm, matrix size = 16 × 16, slice thickness = 6–8 mm, number of echoes = 96, TR = 125 ms, scan time = 0.5 s) with a nominal in-plane resolution of 2.7 mm × 2.7 mm was used for metabolic imaging of hyperpolarized [1-^{13}C]pyruvate and its metabolic products[20,25,31], [1-^{13}C]lactate, [1-^{13}C]alanine, [1-^{13}C]pyruvate hydrate, and ^{13}C-bicarbonate. The ^{13}C transmit RF power was calibrated over the targeted slice using a reference phantom (3.4-M solution of [1-^{13}C]lactate) placed on top of the animal's head. A variable flip angle scheme (four flip angles) was used for constant effective RF excitations between interleaves[32]. Single time-point data were acquired 30 s after the start of the pyruvate injection. The injection-to-scan delay was determined to maximize the lactate and bicarbonate signal detection based on prior dynamic metabolic imaging study[20,31].

To confirm tumor size and location, contrast-enhanced (CE) T_1-weighted proton spin-echo images (axial plane, TE/TR = 12/700 ms, 25 slices, slice thickness = 1 mm, number of excitations = 6, FOV = 87 mm, matrix size = 256 × 256, acquisition time = 9:02 min) were acquired after injecting 0.9 mL of 1:2-mixture of gadolinium-DTPA (Magnevist, Bayer Schering Pharma, Berlin-Wedding, Germany) and saline at the end of each animal's imaging experiment.

Image processing and analysis

All ^{13}C data sets were processed using customized MATLAB® (Mathworks Inc., Natick, MA) scripts. The acquired raw data were apodized by a 10-Hz Gaussian filter and zero-filled by a factor of four both in the time domain and in the spatial dimensions. After a fast Fourier transform (FFT) in the time domain, the chemical shift artifact along the readout direction was corrected [25]. Following gridding onto Cartesian coordinates, a two-dimensional FFT was applied in the two spatial frequency domains. Metabolic maps were calculated by integrating the corresponding metabolite peaks in absorption mode. Metabolite maps and ratios were calculated and normalized relative to spatial maximum signals of pyruvate map and total carbon (tC) map, respectively. The assessment of cerebral metabolism via the region of interest (ROI) comparisons between tumor and normal-appearing brain were performed by spatially averaging each voxel's spectrum followed by peak integrations. The signal-to-noise ratio (SNR) of each metabolite map was measured by dividing the averaged signal in brain by the root mean square (RMS) noise in a background region.

Tumor size measurement

Due to the relatively large ^{13}C CSI voxel size, the measured metabolite maps could suffer from partial volume effects, which might underestimate the tumor lactate-to-bicarbonate ratios, particularly in animals with small tumors. Moreover, some signal contamination between normal-appearing brain and tumor are likely unavoidable due to degradation of the point-spread function caused by blood flow, metabolic conversion, or inconsistent RF excitations between interleaved acquisitions, resulting in possible overestimation of lactate-to-bicarbonate ratio. Thus, we also examined the effects of tumor size on the metabolite ratio both in tumor and normal brain regions. Tumor sizes were measured from the CE T_1-weighted spin echo images using OsiriX and compared with lactate-to-bicarbonate ratio.

Contrast-enhanced T_1-weighted MRI

As a simple DCE MRI surrogate, contrast enhancement on T_1-weighted MRI is widely used in clinical practice to estimate tumor growth as well as overall volume[33]. Averaged signal intensity of tumor ROI was normalized to that of adjacent normal-appearing brain in the CE T_1-weighted ^{1}H spin-echo images to estimate the change of the image contrast between the four groups: baseline, 3 hrs-, 24 hrs-, and 48 hrs-post anti-VEGF treatment.

Histology

After the ^{13}C MRSI experiments, blinded post-mortem histological analysis was performed on excised glioma tissue. Rats were sacrificed 12–24 hrs after imaging via trans-cardiac perfusion with 4-% buffered paraformaldehyde. Brains were extracted and immersed in the same fixative overnight and then cryoprotected up to 30-% buffered sucrose solution before 50-μm sections were made using a sliding frozen microtome. Sections were immune-stained with rabbit anti-phospho-Histone H3 (Ser10, Cell Signaling Technology) antibody. In brief, the floating brain sections were incubated in 1-% H_2O_2 to eliminate endo-peroxidases, in 10-% normal goat serum and 0.1-% Triton-X in tris-buffer to block the non-specific binding, in species compatible biotynlated secondary antibody. 3,3′-Diaminobenzidine (DAB) was used to visualize the end product, after which sections were counterstained with hematoxylin. Adjacent sections were stained with hematoxylin and eosin (H&E) to identify tumor.

Estimation of proliferating cells

Proliferation rate was estimated using a Stereo Investigation System (MicroBrightField, Vermont, USA) connected to an Axioplan light microscope with a motorized stage (Zeiss, Germany). Tumor profile was defined with histone H3 immuno-stained and hematoxylin counterstained sections using the 2.5× objective lens. Sampling was done in 6 tumor-bearing brain sections that were at least 0.6 mm apart to avoid possible over-estimation by counting the same cell more than once. Section thickness was measured and the average of post-histological procedure thickness was manually set at 15 μm (dissector height). The size of the counting frame was set to 250 μm × 250 μm. Counting was performed using the 200× objective lens. The final density of proliferating cells in each tumor was estimated by the ratio of cell numbers and volume of tumor generated by Stereo Investigation Software.

Statistical analysis

All measured metabolite ratios are reported as mean ± standard error. Differences of the lactate/tC, bicarbonate/tC, and lactate/bicarbonate ratios between normal brain and glioma of each treated group were assessed for statistical significance using a paired Student’s t-test with a two-tailed hypothesis ($\alpha = 0.05$) as the two observations are paired. Likewise the metabolic responses of glioma and normal-appearing brain to anti-VEGF treatment (and saline controls) in intra-subject study were also evaluated using the paired Student’s t-test. Metabolite ratios and tumor sizes of untreated and anti-VEGF treated groups (from the group *in vivo* measurements) were analyzed using Mann-Whitney-Wilcoxon test (two-tailed, $\alpha = 0.05$) because each group is independent of the other groups and their distributions are unknown.

Results

Cerebral energy metabolism

Several metabolic products were consistently detected from both healthy and glioma-bearing rat brains after an injection of 125-mM hyperpolarized [1-^{13}C]pyruvate. Spatially averaged spectrum acquired from a representative healthy rat brain (Fig. 1A) shows [1-^{13}C]pyruvate (173.3 ppm, pyruvate/tC = 0.652 ± 0.004, N = 3), [1-^{13}C]lactate (185.5 ppm, lactate/tC = 0.251 ± 0.002), [1-^{13}C]pyruvate hydrate (181.6 ppm, pyruvate hydrate/tC = 0.044 ± 0.006), and ^{13}C-bicarbonate (163.2 ppm, bicarbonate/tC = 0.053 ± 0.002). Lactate-to-bicarbonate ratio was 4.77 ± 0.19. $^{13}CO_2$, which is ~ 10 % of the bicarbonate signal at physiological pH [34] ($pH = pK_a + log_{10}([HCO_3^-]/[CO_2])$), is located outside of the observable spectral window (125 ppm). The corresponding metabolite maps (Fig. 1B–F) and the metabolite maps normalized by tC (Fig. 1G, H) were also reconstructed. Lactate-to-bicarbonate ratios (Fig. 1I) were relatively low in the cortex of the brain[27,31]. Brain SNRs are calculated as 148.8 ± 20.9 for pyruvate, 200.6 ± 31.8 for lactate, 14.2 ± 1.2 for pyruvate hydrate, 70.2 ± 5.0 for bicarbonate maps. Note that the pyruvate maps experience an apparent higher noise level, primarily caused by the artifacts from inflowing pyruvate in the blood and the resulting inconsistencies in the k-space data from different spiral interleaves. [1-^{13}C]alanine (179 ppm, Fig. 1E) was below the noise level in brain as expected due to the low cerebral activity level of alanine aminotransferase[35].

Glioma metabolism

Averaged spectra demonstrated higher lactate (lactate/tC = 0.393 ± 0.022, paired Student's t-test, $P < 4 \times 10^{-6}$, N = 15, Table 1) and lower bicarbonate (bicarbonate/tC = 0.022 ± 0.003, $P < 2 \times 10^{-6}$) labeling in tumor as compared to contralateral normal-appearing brain (lactate/tC = 0.285 ± 0.014, bicarbonate/tC = 0.049 ± 0.003), similar to the previous studies [15,20,36]. The lactate-to-bicarbonate ratio was 22.9 ± 2.5 in glioma and 5.98 ± 0.31 in normal-appearing brain ($P < 6 \times 10^{-6}$). Alternatively, the reciprocal ratio (bicarbonate/lactate) was 0.057 ± 0.010 in glioma and 0.175 ± 0.012 in the normal side of the brain ($P < 3 \times 10^{-6}$).

Metabolic response to anti-VEGF treatment: intra-subject *in vivo* measurement

As shown in a representative tumor-implanted brain (Fig. 2A), the bicarbonate/tC increased to 0.033 ± 0.002 in glioma (P = 0.006, N = 3) and to 0.051 ± 0.003 (P = 0.05) in normal-appearing brain after the anti-VEGF treatment (Fig. 2C, 2F) as compared to the baseline measurement (Table 2). Lactate decreased to 0.34 ± 0.04 (P = 0.05) in glioma but did not change significantly in normal contralateral side (P = 0.7, Fig. 2D, 2G, Table 2). Lactate-to-bicarbonate ratio, however, dramatically decreased from 30.8 ± 4.5 to 10.3 ± 1.2 in glioma (P = 0.04) whereas that in the normal-appearing brain maintained a comparable level: 6.4 ± 0.4 at baseline to 6.0 ± 0.7 after anti-VEGF treatment (P = 0.4, Fig. 2E, 2I). The metabolite ratios were not affected in the saline-injected group (N = 3) both in glioma and in normal-appearing brain (Table 2).

Metabolic response to anti-VEGF treatment: inter-subject *in vivo* measurement

Although small differences in tumor [1-^{13}C]lactate levels could be seen as early as 3 hrs after treatment, detection of metabolic changes were markedly enhanced by incorporating simultaneous changes in ^{13}C-bicarbonate (Mann-Whitney-Wilcoxon u-test, $P < 0.001$, Table 3). Accordingly, intratumoral lactate-to-bicarbonate ratios decreased ($P < 0.001$) to levels approaching the contralateral unaffected side by 3 hrs after drug administration, an effect that is likely too rapid to be explained solely by inhibited angiogenesis. This maximal effect appeared to be transient; lactate/bicarbonate ratios in groups imaged at 24 hrs and 48 hrs after the anti-VEGF treatment increased to 10.6 ± 1.8 and 16.1 ± 4.5, respectively (Fig. 3). Neither bicarbonate nor lactate levels were altered in normal-appearing brain on the contralateral side (Table 3).

Tumor size vs. lactate-to-bicarbonate ratio

The metabolite ratio of lactate-to-bicarbonate in the untreated group 10 days after the tumor implantation showed that there is a moderate correlation (Pearson correlation coefficient, $\rho = 0.54$, $P = 0.04$) between the ratio and the size of tumors (Fig. 4A). In contrast, there was essentially no correlation in normal-appearing brain between tumor sizes and the lactate-to-bicarbonate ratio ($\rho = -0.095$, $P > 0.7$). The tumor sizes of untreated (76.2 ± 13.9 mm^3), and anti-VEGF treated groups at 3 hrs (40.8 ± 22.1 mm^3), 24 hrs (76.0 ± 7.0 mm^3), and 48 hrs (78.3 ± 8.7 mm^3) before the imaging experiments were also not statistically different (Fig. 4B, Mann-Whitney-Wilcoxon u-test, $P > 0.2$). Moreover, no significant reduction or increase of contrast enhancement in glioma, normalized by signals from normal-appearing brain, was observed in the rats treated with anti-VEGF (Fig. 4C): baseline (1.94 ± 0.05), 3 hrs-post (1.81 ± 0.07), 24 hrs-post (1.82 ± 0.02), 48 hrs-post (1.94 ± 0.10).

Proliferating cell density

Proliferation of tumor cells was estimated from histone H3-stained histology. Although the density of proliferating cells of glioma 24–48 hrs (N = 11) after the anti-VEGF treatment tended to be less than that of non-treated glioma tissue (N = 6), the difference was not statistically significant ($P = 0.18$). Representative histone H3-stained glioma tissues from the two groups with the comparable pattern of tumor growth are shown in Figure 5. Histone H3-positive cells are shown as dark brown dots, and a necrotic area is visible on the left side of each section.

Discussion

Cerebral bicarbonate production

This study demonstrates that a robust assessment of bicarbonate as well as lactate production in rat brain is possible after administration of hyperpolarized [1-^{13}C]pyruvate. Administration of a relatively high concentration (125-mM) of pyruvate resulted in increased delivery into brain tissue and higher SNRs of ^{13}C-metabolites compared to those previously reported using 80-mM hyperpolarized [1-^{13}C]pyruvate[37]. The increased SNRs of lactate and bicarbonate in brain can be explained by the transport capacity across the blood-brain barrier of monocarboxylic acids, where the total brain uptake is governed by saturable

(Michaelis-Menten) and non-saturable (free diffusion) components and increases nonlinearly as a function of the concentration of monocarboxylic acid (i.e., pyruvate)[38,39]. This improved visualization enabled consistent measurement of bicarbonate in addition to lactate, thus enabling the opportunity to incorporate bicarbonate measurements into the analysis.

Lactate-to-bicarbonate ratio

Conventionally, studies examining hyperpolarized ^{13}C-substrates have used ratios of [products]-to-[administered substrate] (e.g., [1-^{13}C]lactate-to-[1-^{13}C]pyruvate) or [products]-to-[total ^{13}C-metabolites] as metrics for metabolic assessment, thus compensating the inhomogeneity in tissue perfusion of the infused ^{13}C-substrates. However, these metrics are still sensitive to the injected substrate perfusion, and are subject to corresponding partial volume effects. As an alternative, the ratio of metabolic products is likely a more accurate and quantitative metric being less susceptible to the effects of probe delivery and its membrane transport. Using hyperpolarized [1-^{13}C]pyruvate, [1-^{13}C]lactate-to-^{13}C-bicarbonate ratio (or the reciprocal), as measured by ^{13}C MRS following a bolus injection of hyperpolarized [1-^{13}C]pyruvate, might therefore serve as a better metric to assess the metabolic balance in tumor tissue.

Although the absolute value of the ^{13}C-lactate/^{13}C-bicarbonate ratio is determined by multiple biological factors including LDH and PDH activity, intrinsic ^{12}C-lactate pool size, and availability of nicotinamide adenine dinucleotide (NADH), this metric is sensitive to alterations in the fraction of pyruvate being reduced to lactate versus entering the mitochondria as acetyl-CoA. To the extent that the ^{13}C-labeled acetyl-CoA enters the TCA cycle rather than being metabolized in other pathways, the lactate-to-bicarbonate ratio provides a quantitative tool for assessing changes in the metabolic flux of labeled pyruvate between GLY and OXPHOS. The relatively uniform lactate/bicarbonate distribution over the healthy brain (Fig. 1I) and the increased lactate/bicarbonate in glioma (Fig. 2E) thus suggest spatially homogeneous GLY/OXPHOS in healthy brain and shifted bioenergetics in glioma, respectively.

Tumor metabolism

[1-^{13}C]lactate-to-^{13}C-bicarbonate ratios in glioma were significantly higher than those in normal-appearing brain, consistent with the Warburg effect. Although Warburg originally proposed that a cancer cell's over-utilization of GLY relative to OXPHOS was due to defective mitochondria[11], subsequent studies demonstrated that this excess dependence on the energy-inefficient GLY probably results from a need for carbon skeletons for biomass production[40,41]. By linking increased GLY activity to biomass formation, an interesting corollary can therefore be proposed that forcing an increased rate of OXPHOS relative to GLY should slow or stop growth[43,44]. While this remains to be verified, the capacity to measure this ratio in real time *in situ* using noninvasive, safe technology therefore offers a potentially powerful tool with which to address this relationship.

Anti-VEGF treatment

While it is well known that administration of anti-VEGF therapy is associated with an acute drop tumor blood volume and increased hypoxia[42], there is no information regarding its

impact on tumor tissue metabolism. In this regard, at least two alternative scenarios can be envisioned, one in which metabolism is shifted towards increased glycolysis due to lack of O_2 or, alternatively, a shift towards oxidative metabolism is made due to decreased nutrient delivery. The improved SNRs of [1-^{13}C]pyruvate and downstream products reported in this study enabling consistent measurement of both tumor bicarbonate and lactate offers a way to address this question. Moreover, although potential decreases in blood perfusion might increase metabolite-to-substrate ratios, this is not the case with ratios of produced metabolites (e.g., lactate/bicarbonate), which are relatively perfusion independent[27].

In this model, where administration of a single dose of anti-VEGF antibody produces a 25-% long-term survival rate, the finding of a universal drop in lactate/bicarbonate at 3 hrs is more consistent with the latter shift, i.e., towards oxidative metabolism. Furthermore, it is important to recognize that this measure was primarily dominated by the bicarbonate change, without which no inferences could be made about metabolic dynamics. Consistent with the observation that anti-VEGF therapy has little effect on non-cancerous tissues, this effect was not seen in normal brain, where the ratio is unchanged, and is much too rapid to be explained by inhibition of local vessel formation, thus perhaps reflecting the effect of another property of this pleiotropic molecule[43]. Finally, although not reaching significance, the reduced cell proliferation observed histologically in this study supports the hypothesis that decreased nutrient delivery supports a relationship between the dynamic balance of the metabolic pathways as well as suggesting that a compensatory reliance on OXPHOS might slow tumor growth[44].

Significant tumor shrinkage and marked decrease in contrast agent leakage have been reported several weeks after anti-VEGF treatments in multiple studies[22,33]. We could not, however, detect any change of tumor volume or contrast from CE T_1-weighted MRI over the short duration of the experiment described in this paper. Acute change in vascular permeability was also previously reported[23]. As an alternative of the single time-point imaging, time-resolved imaging of ^{13}C-substrates could be used at the expense of SNR to assess the change in the dynamics of the substrate delivery and enzyme kinetics due to the anti-VEGF treatment[37,45]. Furthermore, co-injection of [1-^{13}C]pyruvate with ^{13}C-urea would provide additional information of permeability, perfusion, and transport[46].

Clinical implication and potential applications

The results observed in this study in the context of anti-VEGF therapy may have clinical relevance, especially if further investigations indicate a relationship between decreasing lactate/bicarbonate and tumor behavior. Furthermore, the robust but transient profound changes in lactate/bicarbonate after anti-VEGF treatment might indicate an early “window of opportunity” for amplifying anti-angiogenic therapies with agents that increase oxidative stress because high rates of OXPHOS occurring in hypoxic environments should result in high concentrations of reactive oxygen species. The feasibility of using the large pyruvate dose (1 mmol/kg vs. 98.9 μmol/kg in the recent human study[47]), however, should be further examined before clinical translation.

Furthermore, since several brain diseases are characterized by mitochondrial dysfunction, the assessment of cerebral mitochondrial activity and PDH flux should be helpful in the

investigation of other types of brain pathology. For example, the lactate-to-bicarbonate ratio from hyperpolarized [1-^{13}C]pyruvate MRS might represent a potentially very useful tool with which to study metabolism of diverse brain diseases such as neurodegenerative diseases[48].

Conclusions

Measurements of both ^{13}C-bicarbonate and [1-^{13}C]lactate production in rat brain following a bolus injection of 125-mM hyperpolarized [1-^{13}C]pyruvate enables ^{13}C-bicarbonate measurement to be incorporated into data analysis. Using a ^{13}C-lactate to bicarbonate ratio, we also demonstrate a rapid and robust decrease in response to anti-angiogenic treatment. The acute changes in lactate/bicarbonate after anti-VEGF therapy suggest a potential application for this technology as a biomarker that can be used to assess effectiveness of not only anti-angiogenic but also other metabolic therapies.

Acknowledgments

Funding: National Institutes of Health (CA176836, EB009070, AA005965, AA0018681, AA13521-INIA, S10 OD012283, P41 EB015891) and the Department of Defense (PC100427) of the United States. We also thank Richard M. Lucas Center, GE Healthcare, Stanford Bio-X Interdisciplinary Initiatives Program, Stanford Radiology Postdoctoral Research Fund, and Nadia's Gift.

Abbreviations

GLY	glycolysis
OXPHOS	oxidative phosphorylation
DNP	dynamic nuclear polarization
PDH	pyruvate dehydrogenase
PDK	pyruvate dehydrogenase kinase
LDH	lactate dehydrogenase
VEGF	vascular endothelial growth factor
ROI	region of interest
tC	total carbon
NADH	nicotinamide adenine dinucleotide
TCA	tricarboxylic acid
FSE	fast spin echo
CSI	chemical shift imaging
FOV	field of view
FFT	fast Fourier transform
MNU	N-methyl-N-nitrosourea
DCE	dynamic contrast enhancement

References

1. Ardenkjaer-Larsen JH, Fridlund B, Gram A, Hansson G, Hansson L, Lerche MH, Servin R, Thaning M, Golman K. Increase in signal-to-noise ratio of > 10,000 times in liquid-state NMR. Proc Natl Acad Sci USA. 2003; 100:10158–10163. [PubMed: 12930897]
2. Golman K, Ardenkjaer-Larsen JH, Petersson JS, Mansson S, Leunbach I. Molecular imaging with endogenous substances. Proc Natl Acad Sci USA. 2003; 100:10435–10439. [PubMed: 12930896]
3. Golman K, in 't Zandt R, Thaning M. Real-time metabolic imaging. Proc Natl Acad Sci USA. 2006; 103:11270–11275. [PubMed: 16837573]
4. Hurd RE, Yen Y-F, Tropp J, Pfefferbaum A, Spielman DM, Mayer D. Cerebral dynamics and metabolism of hyperpolarized [1-13C]pyruvate using time-resolved MR spectroscopic imaging. J Cereb Blood Flow Metab. 2010; 30:1734–1741. [PubMed: 20588318]
5. Schroeder MA, Cochlin LE, Heather LC, Clarke K, Radda GK, Tyler DJ. In vivo assessment of pyruvate dehydrogenase flux in the heart using hyperpolarized carbon-13 magnetic resonance. Proc Natl Acad Sci USA. 2008; 105:12051–12056. [PubMed: 18689683]
6. Spielman DM, Mayer D, Yen Y-F, Tropp J, Hurd RE, Pfefferbaum A. In vivo measurement of ethanol metabolism in the rat liver using magnetic resonance spectroscopy of hyperpolarized [1-13C]pyruvate. Magn Reson Med. 2009; 62:307–313. [PubMed: 19526498]
7. Hurd RE, Spielman D, Josan S, Yen Y-F, Pfefferbaum A, Mayer D. Exchange-linked dissolution agents in dissolution-DNP (13)C metabolic imaging. Magn Reson Med. 2013; 70:936–942. [PubMed: 23165935]
8. Dwyer, D., editor. Glucose Metabolism in the Brain. Academic Press; 2002.
9. Marquis NR, Frits IB. The distribution of carnitine, acetylcarnitine, and carnitine acetyltransferase in rat tissues. J Biol Chem. 1965; 240:2193–2196. [PubMed: 14299646]
10. Park JM, Josan S, Grafendorfer T, Yen Y-F, Hurd RE, Spielman DM, Mayer D. Measuring mitochondrial metabolism in rat brain in vivo using MR Spectroscopy of hyperpolarized [2-^{13}C]pyruvate. NMR Biomed. 2013; 26:1197–1203. [PubMed: 23553852]
11. Warburg O. On the origin of cancer cells. Science. 1956; 123:309–314. [PubMed: 13298683]
12. Gatenby RA, Gillies RJ. Why do cancers have high aerobic glycolysis? Nat Rev Cancer. 2004; 4:891–899. [PubMed: 15516961]
13. Albers MJ, Bok R, Chen AP, Cunningham CH, Zierhut ML, Zhang VY, Kohler SJ, Tropp J, Hurd RE, Yen Y-F, Nelson SJ, Vigneron DB, Kurhanewicz J. Hyperpolarized 13C lactate, pyruvate, and alanine: noninvasive biomarkers for prostate cancer detection and grading. Cancer Res. 2008; 68:8607–8615. [PubMed: 18922937]
14. Day SE, Kettunen MI, Gallagher FA, Hu D-E, Lerche M, Wolber J, Golman K, Ardenkjaer-Larsen JH, Brindle KM. Detecting tumor response to treatment using hyperpolarized 13C magnetic resonance imaging and spectroscopy. Nat Med. 2007; 13:1382–1387. [PubMed: 17965722]
15. Chaumeil MM, Ozawa T, Park I, Scott K, James CD, Nelson SJ, Ronen SM. Hyperpolarized 13C MR spectroscopic imaging can be used to monitor Everolimus treatment in vivo in an orthotopic rodent model of glioblastoma. Neuroimage. 2012; 59:193–201. [PubMed: 21807103]
16. Bohndiek SE, Kettunen MI, Hu D-E, Brindle KM. Hyperpolarized (13)C spectroscopy detects early changes in tumor vasculature and metabolism after VEGF neutralization. Cancer Res. 2012; 72:854–864. [PubMed: 22223844]
17. Park I, Bok R, Ozawa T, Phillips JJ, James CD, Vigneron DB, Ronen SM, Nelson SJ. Detection of early response to temozolomide treatment in brain tumors using hyperpolarized 13C MR metabolic imaging. J Magn Reson Imaging. 2011; 33:1284–1290. [PubMed: 21590996]
18. Maher EA, Marin-Valencia I, Bachoo RM, Mashimo T, Raisanen J, Hatanpaa KJ, Jindal A, Jeffrey FM, Choi C, Madden C, Mathews D, Pascual JM, Mickey BE, Malloy CR, DeBerardinis RJ. Metabolism of [U-13 C]glucose in human brain tumors in vivo. NMR Biomed. 2012; 25:1234–1244. [PubMed: 22419606]
19. Day SE, Kettunen MI, Cherukuri MK, Mitchell JB, Lizak MJ, Morris HD, Matsumoto S, Koretsky AP, Brindle KM. Detecting response of rat C6 glioma tumors to radiotherapy using hyperpolarized [1-13C]pyruvate and 13C magnetic resonance spectroscopic imaging. Magn Reson Med. 2011; 65:557–563. [PubMed: 21264939]

20. Park JM, Recht LD, Josan S, Merchant M, Jang T, Yen Y-F, Hurd RE, Spielman DM, Mayer D. Metabolic response of glioma to dichloroacetate measured in vivo by hyperpolarized (13)C magnetic resonance spectroscopic imaging. Neuro-oncology. 2013; 15:433–441. [PubMed: 23328814]
21. Stacpoole PW. The pharmacology of dichloroacetate. Metabolism. 1989; 38:1124–1144. [PubMed: 2554095]
22. Keunen O, Johansson M, Oudin A, Sanzey M, Rahim SAA, Fack F, Thorsen F, Taxt T, Bartos M, Jirik R, Miletic H, Wang J, Stieber D, Stuhr L, Moen I, Rygh CB, Bjerkvig R, Niclou SP. Anti-VEGF treatment reduces blood supply and increases tumor cell invasion in glioblastoma. Proc Natl Acad Sci USA. 2011; 108:3749–3754. [PubMed: 21321221]
23. Raatschen H-J, Simon GH, Fu Y, Sennino B, Shames DM, Wendland MF, McDonald DM, Brasch RC. Vascular permeability during antiangiogenesis treatment: MR imaging assay results as biomarker for subsequent tumor growth in rats. Radiology. 2008; 247:391–399. [PubMed: 18372448]
24. Baumgarten von L, Brucker D, Tirniceru A, Kienast Y, Grau S, Burgold S, Herms J, Winkler F. Bevacizumab has differential and dose-dependent effects on glioma blood vessels and tumor cells. Clin Cancer Res. 2011; 17:6192–6205. [PubMed: 21788357]
25. Mayer D, Yen Y-F, Tropp J, Pfefferbaum A, Hurd RE, Spielman DM. Application of subsecond spiral chemical shift imaging to real-time multislice metabolic imaging of the rat in vivo after injection of hyperpolarized 13C1-pyruvate. Magn Reson Med. 2009; 62:557–564. [PubMed: 19585607]
26. Chronik BA, Alejski A, Rutt BK. Design and fabrication of a three-axis multilayer gradient coil for magnetic resonance microscopy of mice. Magn Reson Med. 2000; 44:955–963. [PubMed: 11108634]
27. Josan S, Hurd R, Billingsley K, Senadheera L, Park JM, Yen Y-F, Pfefferbaum A, Spielman D, Mayer D. Effects of isoflurane anesthesia on hyperpolarized (13)C metabolic measurements in rat brain. Magn Reson Med. 2013; 70:1117–1124. [PubMed: 23086864]
28. Benda P, Lightbody J, Sato G, Levine L, Sweet W. Differentiated rat glial cell strain in tissue culture. Science. 1968; 161:370–371. [PubMed: 4873531]
29. Liang W-C, Wu X, Peale FV, Lee CV, Meng YG, Gutierrez J, Fu L, Malik AK, Gerber H-P, Ferrara N, Fuh G. Cross-species vascular endothelial growth factor (VEGF)-blocking antibodies completely inhibit the growth of human tumor xenografts and measure the contribution of stromal VEGF. J Biol Chem. 2006; 281:951–961. [PubMed: 16278208]
30. Fuh G, Wu P, Liang W-C, Ultsch M, Lee CV, Moffat B, Wiesmann C. Structure-function studies of two synthetic anti-vascular endothelial growth factor Fabs and comparison with the Avastin Fab. J Biol Chem. 2006; 281:6625–6631. [PubMed: 16373345]
31. Mayer D, Yen Y-F, Takahashi A, Josan S, Tropp J, Rutt BK, Hurd RE, Spielman DM, Pfefferbaum A. Dynamic and high-resolution metabolic imaging of hyperpolarized [1-13C]-pyruvate in the rat brain using a high-performance gradient insert. Magn Reson Med. 2011; 65:1228–1233. [PubMed: 21500253]
32. Zhao L, Mulkern R, Tseng CH, Williamson D, Patz S, Kraft R, Walsworth RL, Jolesz FA, Albert MS. Gradient-echo imaging considerations for hyperpolarized 129Xe MR. J Magn Reson B. 1996; 113:179–183.
33. Jalali S, Chung C, Foltz W, Burrell K, Singh S, Hill R, Zadeh G. MRI biomarkers identify the differential response of glioblastoma multiforme to anti-angiogenic therapy. Neuro-oncology. 2014; 16:868–879. [PubMed: 24759636]
34. Gallagher FA, Kettunen MI, Day SE, Hu D-E, Ardenkjaer-Larsen JH, Zandt RI, Jensen PR, Karlsson M, Golman K, Lerche MH, Brindle KM. Magnetic resonance imaging of pH in vivo using hyperpolarized 13C-labelled bicarbonate. Nature. 2008; 453:940–943. [PubMed: 18509335]
35. Erakovic V, Zupan G, Varljen J, Laginja J, Simonic A. Altered activities of rat brain metabolic enzymes in electroconvulsive shock-induced seizures. Epilepsia. 2001; 42:181–189. [PubMed: 11240587]

36. Park I, Larson PEZ, Zierhut ML, Hu S, Bok R, Ozawa T, Kurhanewicz J, Vigneron DB, Vandenberg SR, James CD, Nelson SJ. Hyperpolarized 13C magnetic resonance metabolic imaging: application to brain tumors. Neuro-oncology. 2010; 12:133–144. [PubMed: 20150380]
37. Park JM, Josan S, Jang T, Merchant M, Yen Y-F, Hurd RE, Recht L, Spielman DM, Mayer D. Metabolite kinetics in C6 rat glioma model using magnetic resonance spectroscopic imaging of hyperpolarized [1-(13)C]pyruvate. Magn Reson Med. 2012; 68:1886–1893. [PubMed: 22334279]
38. Hurd RE, Yen Y-F, Mayer D, Chen A, Wilson D, Kohler S, Bok R, Vigneron D, Kurhanewicz J, Tropp J, Spielman D, Pfefferbaum A. Metabolic imaging in the anesthetized rat brain using hyperpolarized [1-13C] pyruvate and [1-13C] ethyl pyruvate. Magn Reson Med. 2010; 63:1137–1143. [PubMed: 20432284]
39. Cremer JE, Cunningham VJ. Kinetics of blood-brain barrier transport of pyruvate, lactate and glucose in suckling, weanling and adult rats. J Neurochem. 1979; 33:439–445. [PubMed: 469534]
40. Vander Heiden MG, Cantley LC, Thompson CB. Understanding the Warburg effect: the metabolic requirements of cell proliferation. Science. 2009; 324:1029–1033. [PubMed: 19460998]
41. Vander Heiden MG, Lunt SY, Dayton TL, Fiske BP, Israelsen WJ, Mattaini KR, Vokes NI, Stephanopoulos G, Cantley LC, Metallo CM, Locasale JW. Metabolic pathway alterations that support cell proliferation. Cold Spring Harb Symp Quant Biol. 2011; 76:325–334. [PubMed: 22262476]
42. Miyazaki S, Kikuchi H, Iino I, Uehara T, Setoguchi T, Fujita T, Hiramatsu Y, Ohta M, Kamiya K, Kitagawa K, Kitagawa M, Baba S, Konno H. Anti-VEGF antibody therapy induces tumor hypoxia and stanniocalcin 2 expression and potentiates growth of human colon cancer xenografts. Int J Cancer. 2014; 135:295–307. [PubMed: 24375080]
43. Goel HL, Mercurio AM. VEGF targets the tumour cell. Nat Rev Cancer. 2013; 13:871–882. [PubMed: 24263190]
44. Thomas, P.; Spielman, D.; Recht, L. The Bevacizumab “Pseudoresponse” in Glioma: Disappointment or Opportunity?. In: Abujamra, AL., editor. Brain tumors - current and emerging therapeutic strategies. InTech; 2011. p. 53-66.
45. Schroeder MA, Ali MA, Hulikova A, Supuran CT, Clarke K, Vaughan-Jones RD, Tyler DJ, Swietach P. Extramitochondrial domain rich in carbonic anhydrase activity improves myocardial energetics. Proc Natl Acad Sci USA. 2013; 110:E958–67. [PubMed: 23431149]
46. Morze Von C, Bok RA, Reed GD, Ardenkjaer-Larsen JH, Kurhanewicz J, Vigneron DB. Simultaneous multiagent hyperpolarized (13)C perfusion imaging. Magn Reson Med. 2014; 72:1599–1609. [PubMed: 24382698]
47. Nelson SJ, Kurhanewicz J, Vigneron DB, Larson PEZ, Harzstark AL, Ferrone M, Van Criekinge M, Chang JW, Bok R, Park I, Reed G, Carvajal L, Small EJ, Munster P, Weinberg VK, Ardenkjaer-Larsen JH, Chen AP, Hurd RE, Odegardstuen L-I, Robb FJ, Tropp J, Murray JA. Metabolic imaging of patients with prostate cancer using hyperpolarized [1-^{13}C]pyruvate. Sci Transl Med. 2013; 5:198ra108.
48. Lin MT, Beal MF. Mitochondrial dysfunction and oxidative stress in neurodegenerative diseases. Nature. 2006; 443:787–795. [PubMed: 17051205]

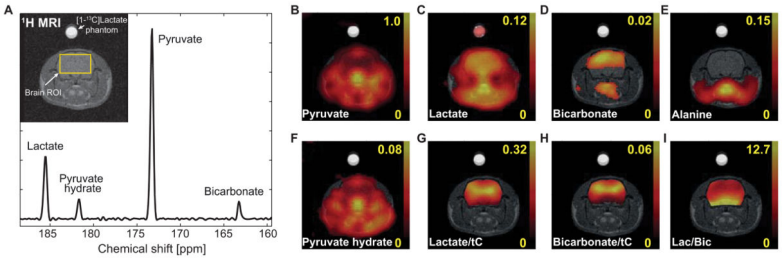

Figure 1.

^{13}C MRS data acquired from a representative healthy rat after an administration of 125-mM hyperpolarized [1-^{13}C]pyruvate; (**A**) Spectrum averaged over the brain ROI shown in the ^{1}H MRI. Metabolite maps of (**B**) [1-^{13}C]pyruvate, (**C**) [1-^{13}C]lactate, (**D**) ^{13}C-bicarbonate, (**E**) [1-^{13}C]alanine, and (**F**) [1-^{13}C]pyruvate hydrate scaled by the maximum pyruvate signal. Maps of (**G**) lactate-to-tC, (**H**) bicarbonate-to-tC, and (**I**) Lactate-to-bicarbonate ratio map. The tC map calculated as the sum of all metabolite maps. Brain masking was applied for ^{13}C map in **G–I**. The yellow numbers next to color bars represent relative scale of each metabolite map to the maximum pyruvate signal (**B–F**) or metabolite ratios (**G–I**).

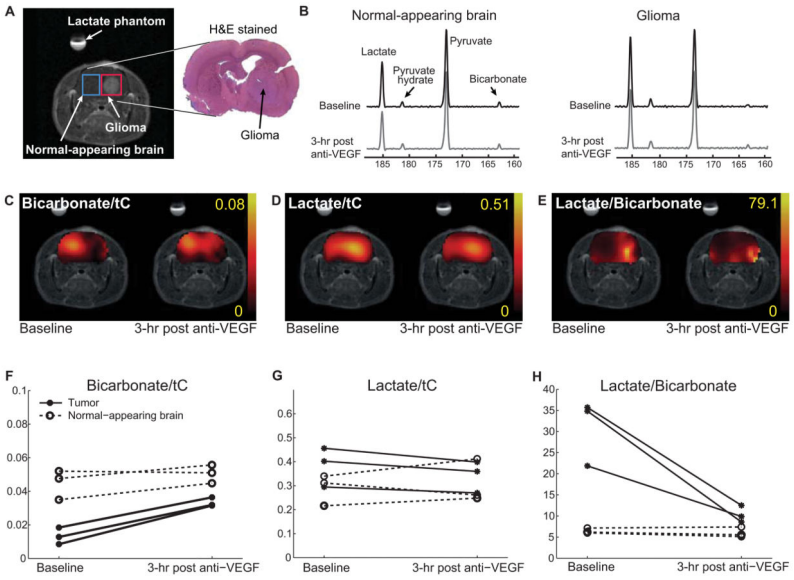

Figure 2.

Intra-subject metabolic changes after an anti-VEGF mab administration measured by hyperpolarized [1-^{13}C]pyruvate MRS. (**A**) ROIs for glioma (red) and normal-appearing brain (blue) were selected based on the contrast-enhanced (gadolinium) T_1-weighted images. The hyper-intense region within brain denotes tumor, which can be also confirmed from the matching slice of the H&E-stained histology. (**B**) Relative changes in ^{13}C MRS spectra of the normal-appearing and glioma ROIs acquired from a representative rat before and 3 hrs after a single anti-VEGF treatment. (**C**) Representative bicarbonate-to-tC map showed a dramatic increase in glioma after the treatment (brain masking used). (**D**) Lactate in glioma decreased mildly after the treatment. (**E**) Lactate-to-bicarbonate ratio drastically decreased in glioma after the treatment (P = 0.04) while no significant change was observed in contralateral normal-appearing brain (P = 0.4). Comparison of (**F**) bicarbonate/tC, (**G**) lactate/tC, and (**H**) lactate/bicarbonate from individual rats (N = 3) before and after anti-VEGF treatment.

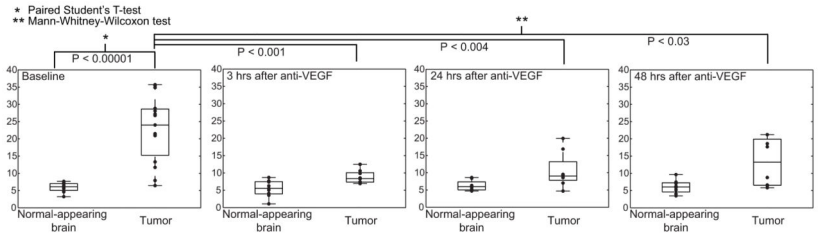

Figure 3.

Difference in lactate-to-bicarbonate ratio in untreated and treated rats at 3 hrs, 24 hrs, and 48 hrs after a single injection of anti-VEGF mab (5 mg/kg). The metabolite ratio decreased from 23.6 ± 2.3 (N = 15) in the untreated group to 8.9 ± 0.6 (N = 9) for 3 hrs-post treatment group in the tumor, and increased back to 10.6 ± 1.8 (N = 8) and 16.1 ± 4.5 (N = 8) in the 24 hrs- and 48 hrs-post treatment groups, respectively. Bicarbonate, lactate, and lactate-to-bicarbonate levels were not significantly altered in contralateral normal-appearing brain; Lactate-to-bicarbonate ratio = 6.0 ± 0.3 (untreated), 5.6 ± 0.8 (3 hrs), 6.2 ± 0.5 (24 hrs), 6.1 ± 0.7 (48 hrs).

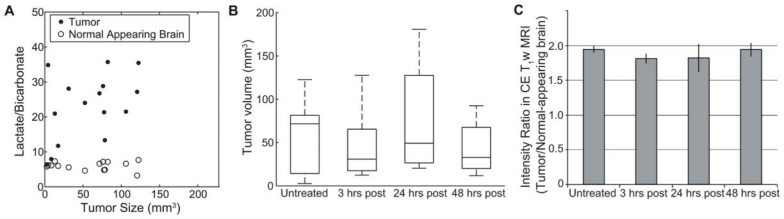

Figure 4.

Effect of tumor size on lactate-to-bicarbonate ratios. (**A**) Correlation between lactate-to-bicarbonate ratio and tumor volume in untreated group (N = 15) at day 10 after glioma-implantation was moderate ($\rho = 0.54$, $P = 0.04$). The tumor sizes were measured based on the hyper-intense regions of the contrast-enhanced T_1-weighted proton MRI. Lactate-to-bicarbonate ratio from the contralateral normal-appearing brain ROIs was not also affected by tumor sizes ($\rho = -0.095$, $P > 0.7$). (**B**) The tumor sizes and (**C**) the contrast enhancement of untreated and anti-VEGF treated groups at 3 hrs, 24 hrs, and 48 hrs before the imaging experiments showed no significant difference between any pair of the groups.

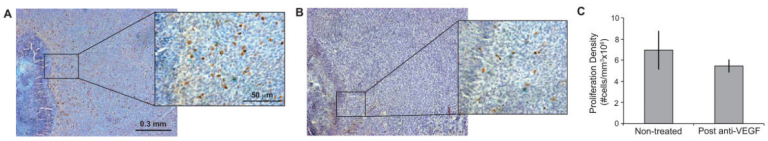

Figure 5.

Representative histone H3-stained histology of glioma from (A) a non-treated rat and (B) an anti-VEGF-treated rat. Tumors with comparable pattern of tumor growth are presented. Histone H3-positive cells shown as dark dots indicate proliferating cells, and a necrotic area is visible on the left side of each section. (C) The average density of proliferating cells of glioma was lower (P = 0.18) in anti-VEGF-treated tumors (N = 11, 24–48 hrs post treatment) than in non-treated group (N = 6).

Table 1

Metabolic ratios in brain measured using 125-mM hyperpolarized [1-^{13}C]pyruvate

Higher lactate and lower bicarbonate labeling, thus larger lactate-to-bicarbonate ratio, in tumor as compared to contralateral normal-appearing brain were measured.

	Healthy brain (N = 3)	Glioma-implanted brain (N = 15)	
		Glioma	Normal-appearing brain
Pyruvate hydrate/tC	0.044 ± 0.006	0.058 ± 0.013	0.053 ± 0.006
Bicarbonate/tC	0.053 ± 0.002	0.022 ± 0.003 *	0.049 ± 0.003
Lactate/tC	0.251 ± 0.002	0.393 ± 0.022 *	0.285 ± 0.014
Lactate/Bicarbonate	4.77 ± 0.19	22.9 ± 2.5 *	5.98 ± 0.31

Values are means + standard errors.

*indicates significant difference between glioma and normal-appearing brain ($P < 10^{-5}$, two-tailed paired Student's t-test).

Table 2

Intra-subject changes of hyperpolarized MR metabolite ratios in anti-VEGF drug- and saline-treated groups

Bicarbonate was increased both in glioma (P = 0.006) and normal-appearing brain (P = 0.05) 3 hrs after the anti-VEGF treatment. Lactate slightly decreased in glioma (P = 0.05) whereas no significant difference was detected in normal-appearing brain. While unaffected in normal-appearing brain, lactate-to-bicarbonate ratio decreased dramatically in glioma (P = 0.04).

	Group treated with anti-VEGF drug (N = 3)				Control group treated with saline (N = 3)			
	Glioma		Normal-appearing brain		Glioma		Normal-appearing brain	
	Baseline	3 hrs post	Baseline	3 hrs post	Baseline	3 hrs post	Baseline	3 hrs post
Bicarbonate/tC	0.013 ± 0.003	0.033 ± 0.002 **	0.045 ± 0.005	0.051 ± 0.003	0.016 ± 0.003	0.017 ± 0.003	0.050 ± 0.002	0.056 ± 0.005
Lactate/tC	0.38 ± 0.05	0.34 ± 0.04	0.29 ± 0.04	0.31 ± 0.05	0.35 ± 0.03	0.35 ± 0.02	0.29 ± 0.01	0.28 ± 0.01
Lactate/Bicarbonate	30.8 ± 4.5	10.3 ± 1.2 *	6.4 ± 0.4	6.0 ± 0.7	24.7 ± 5.3	22.1 ± 5.2	5.8 ± 0.1	5.1 ± 0.6

Values are means + standard errors.

*and ** indicate significant change (P < 0.05 and P < 0.01, respectively) due to anti-VEGF drug (two-tailed Student's paired t-test).

Table 3

Group *in vivo* measurements of hyperpolarized MR metabolite ratios after anti-VEGF treatment

Intratumoral lactate-to-bicarbonate ratios decreased to levels approaching the contralateral side by 3 hrs after anti-VEGF treatment, and gradually increased when measured at 24 hrs and 48 hrs post-treatment. Lactate-to-bicarbonate ratio of normal-appearing brain was similar across all groups.

	Glioma				Normal-appearing brain			
	Baseline (N = 15)	**3 hrs post (N = 9)**	**24 hrs post (N = 8)**	**48 hrs post (N = 8)**	**Baseline**	**3 hrs post**	**24 hrs post**	**48 hrs post**
Bicarbonate/tC	0.021 ± 0.003	0.038 ± 0.003***	0.032 ± 0.005*	0.03 ± 0.01*	0.049 ± 0.003	0.051 ± 0.004	0.048 ± 0.005	0.037 ± 0.006
Lactate/tC	0.39 ± 0.02	0.33 ± 0.02*	0.332 ± 0.034	0.344 ± 0.076	0.29 ± 0.01	0.28 ± 0.04	0.29 ± 0.02	0.21 ± 0.02
Lactate/Bicarbonate	23.6 ± 2.3	8.9 ± 0.6***	10.6 ± 1.8**	16.1 ± 4.5*	6.0 ± 0.3	5.6 ± 0.8	6.3 ± 0.5	6.1 ± 0.70

Values are means + standard errors.

*, **, ***indicate significant difference (P < 0.05, P < 0.01, P < 0.001, respectively) of post-treatment from the baseline (Mann-Whitney-Wilcoxon u-test).